



Novel coumarin rhenium(I) and -(V) complexes: Formation, DFT and DNA binding studies

Barushka Jadoo^a, Irvin Noel Booyesen^{a,*}, Matthew Piers Akerman^a, Lydia Rhyman^{b,c}, Ponnadurai Ramasami^{b,c}

^aSchool of Chemistry and Physics, University of KwaZulu-Natal, Private Bag X01, Scottsville, 3209 Pietermaritzburg, South Africa

^bComputational Chemistry Group, Department of Chemistry, Faculty of Science, University of Mauritius, Réduit, 80837, Mauritius

^cDepartment of Applied Chemistry, University of Johannesburg, Doornfontein Campus, Johannesburg 2028, South Africa

ARTICLE INFO

Article history:

Received 29 November 2017

Accepted 18 January 2018

Available online 31 January 2018

Keywords:

Rhenium

Coumarin

DNA binding

DFT

Spectral characterization

ABSTRACT

Herein, we report the formation and characterisation of novel rhenium(I) and -(V) compounds with coumarin bidentate chelates: *trans*-[ReOBr₂(PPh₃)(hbc)] (**1**) (Hhbc = 7-(2-hydroxybenzylideneamino)-4-(trifluoromethyl)-2H-chromen-2-one), *fac*-[Re(CO)₃Cl(aomc)] (**2**) (aomc = 7-(((2-amino-4-oxo-4H-chromen-3-yl)methylene)amino)-4-(trifluoromethyl)-2H-chromen-2-one) and *fac*-[Re(CO)₃Cl(moac)] (**3**) (moac = 7-(((2-methoxy-4-oxochroman-3-yl)methylene)amino)-4-(trifluoromethyl)-2H-chromen-2-one). The coumarin free-ligands and the metal complexes **1–3** were characterized by NMR, UV–Vis and FTIR spectroscopy, melting point and molar conductivity measurements as well as time-of-flight mass spectrometry. Their structural elucidations were supported by the respective solid state structures of **1**, Hhbc and moac. DNA binding studies conducted using the *facial* tricarbonylrhenium(I) complexes **2** and **3**, revealed that they are DNA groove binders with intrinsic binding constants in the order of 10⁵ and 10⁴ M bp, respectively. This study was also complemented using density functional theory (DFT) and time-dependent DFT methods to attain a deeper understanding into the structural parameters, infrared and electronic spectra of these coumarin free-ligands and their metal complexes **1–3**.

© 2018 Elsevier Ltd. All rights reserved.

1. Introduction

The design of new target-specific rhenium radiopharmaceuticals necessitates exploring the coordination susceptibility of rhenium towards multidentate chelators encompassing various biologically relevant moieties [1,2]. Rhenium naturally occurs as a mixture of two non-radioactive isotopes ¹⁸⁵Re and ¹⁸⁷Re while the rhenium radionuclides used in nuclear medicine are ¹⁸⁶Re and ¹⁸⁸Re have β -emission energies and half-lives adequate for therapeutic treatment of cancer [3,4]. Schiff bases have shown to exhibit high coordination affinities towards rhenium(I) and -(V) cores and moreover, their metal complexes have shown to exhibit a wide array of physical properties culminating into applications including chemical sensing, DNA interaction, cell imaging and catalysis [5–8].

Recent studies shows that transition metal complexes with chromone Schiff base chelates have been isolated and many of these metal complexes have shown optimal *in vitro* anticancer

activities [9]. However, the formation of coumarin Schiff bases remains relatively unexplored despite the facts that the isostructural benzopyranes; coumarin and chromones are secondary metabolites and that they are building blocks of various drugs [10]. Among the few examples of *d*-block metal complexes of coumarin Schiff bases include the [M(II)(L)2H₂O] {M = Ni, Cu or Co} complexes (L = (*E*)-*N*-(3-chlorophenyl)-2-(1-(7-hydroxy-4-methyl-2-oxo-2H-chromen-8-yl)ethylidene)hydrazinocarbothioamide) where a synergistic effect is observed based on the higher antimicrobial effects of the metal complexes compared to their free-ligands [11].

A combination drug, coumarin/troloxerutine have shown therapeutic application in the perseverance of the salivary glands and mucosa in patients who underwent head and neck radiotherapy [12]. The results also suggest that the co-drug, coumarin has a defined biodistribution pattern and this provides impetus in developing coumarin Schiff base rhenium compounds which can be potential therapeutic radiopharmaceutical for salivary gland cancer. In this research study, we report the formation of [Re^{VO}]³⁺ and *fac*-[Re^I(CO)₃]⁺ compounds with bidentate coumarin ligands derived from 7-amino-4-(trifluoromethyl)coumarin. The rhenium complexes, *trans*-[ReOBr₂(PPh₃)(hbc)] (**1**), *cis*-[Re(CO)₃Cl(aomc)] (**2**) and *cis*-[Re(CO)₃Cl(moac)] (**3**) were each synthesized from the

* Corresponding author. Fax: +27 33 260 5009.

E-mail address: Booyeni@ukzn.ac.za (I.N. Booyesen).

coordination reactions of rhenium(V) and -(I) precursors with the coumarin free-ligands: 7-(2-hydroxybenzylideneamino)-4-(trifluoromethyl)-2H-chromen-2-one (Hhbc), 7-(((2-amino-4-oxo-4H-chromen-3-yl)methylene)amino)-4-(trifluoromethyl)-2H-chromen-2-one (aomc) and 7-(((2-methoxy-4-oxochroman-3-yl)methylene)amino)-4-(trifluoromethyl)-2H-chromen-2-one (moac), respectively (see Fig. 1). Furthermore, a detailed understanding of the electronic structures and spectroscopic properties are important to aid in the interpretation of the experimental findings. There are reports on the use of density functional theory (DFT) methods to complement experimental research involving rhenium(I) [13] and -(V) complexes [14]. Consequently, computational methods were employed to aid in the interpretation of experimental data.

2. Experimental

2.1. Materials and methods

The following chemicals: 7-amino-4-(trifluoromethyl)-coumarin, salicylaldehyde, 3-formylchromone, 2-amino-3-formylchromone, pentacarbonylchlororhenium(I), calf thymus DNA (CT-DNA) and phosphate buffered saline (PBS) tablets were purchased from Sigma-Aldrich and used as received. The oxorhenium(V) precursors were synthesized *via* methods obtained from literature [15,16]. All solvents were obtained from Merck SA. Reagent grade toluene was dried over sodium wire while other solvents and chemicals were used without any further purification. Ultrapure water was produced from an Elga Purelab Ultra system. Infrared spectra (IR) were recorded on a Perkin Elmer Spectrum 100 spectrometer in the 4000–200 cm^{-1} range. The IR spectra of all the compounds were attained in the solid state using the Perkin Elmer Universal ATR Accessory (UATR). The ^1H and ^{13}C NMR spectra were obtained at 295 K using a Bruker Avance 400 or 500 MHz spectrometer. All NMR spectra were recorded in DMSO- d_6 . UV-Vis spectra were recorded using a Perkin Elmer Lambda 25 spectrometer. The extinction coefficients (ϵ) are given in $\text{dm}^3 \text{mol}^{-1} \text{cm}^{-1}$. The melting points were obtained using a Stuart SMP3 apparatus. The conductivity measurements were determined at 295 K on a Radiometer R21M127 CD 230 conductivity and pH meter. Mass spectrometry was conducted in both the positive and negative

modes *via* direct injection of the samples into a Waters Micromass LCT Premier mass spectrometer equipped with an electrospray ionization (ESI) source and a time-of-flight (TOF) mass analyser.

2.2. Synthesis of ligands

2.2.1. 7-(2-Hydroxybenzylideneamino)-4-(trifluoromethyl)-2H-chromen-2-one (Hhbc)

The two reactants, 7-amino-4-(trifluoromethyl)coumarin (0.3305 g; 1.440 mmol) and salicylaldehyde (0.15 cm^3 ; 1.440 mmol) were heated until reflux in methanol (20 cm^3) for 3 h. The resultant yellow solution was allowed cool down to room temperature and afterwards further cooled down in an ice bath which resulted in the formation of orange crystals. These crystals were filtered, washed with methanol and petroleum ether. Yield = 50%; Melting point: 189.5–191.6 $^\circ\text{C}$; Infrared ($\nu_{\text{max}}/\text{cm}^{-1}$): $\nu(\text{O}-\text{H})$ 3109 (br, w), $\nu(\text{C}=\text{O})$ 1730 (s), $\nu(\text{C}=\text{N})$ 1595 (s), $\nu(\text{C}-\text{O}-\text{C})$ 1268 (s); ^1H NMR (d_6 -DMSO/295 K/ppm): 12.37 (s, 1H, OH), 9.07 (s, 1H, H11), 7.80–7.71 (m, 2H, H13, H15), 7.62–7.60 (d, $J = 2.0$ Hz, 1H, H9), 7.51–7.44 (m, 2H, H6, H8), 7.05–6.97 (t, $J = 9.0$ Hz, 3H, H3, H14, H16); ^{13}C NMR (d_6 -DMSO/295 K/ppm): 165.55 (C17), 160.36 (C4), 159.35 (C11), 156.54 (C2), 154.84 (C7), 154.07 (C5), 152.70 (C15), 134.22 (C13), 132.49 (C9), 125.72 (C1), 125.70 (C14), 119.35 (C10), 116.77 (C8), 112.18 (C12), 109.44 (C16), 101.72 (C6), 98.95 (C3); UV-Vis (Methanol, λ_{max} (ϵ , $\text{M}^{-1} \text{cm}^{-1}$): 373 nm (36997), 277 nm (sh, 10671), 232 nm (24033); TOF-MS (m/z): Calcd: 333.0613, Found: 332.0537 $[\text{M}-\text{H}]^-$, 333.0613 $[\text{M}]^-$.

2.2.2. 7-(((2-Amino-4-oxo-4H-chromen-3-yl)methylene)amino)-4-(trifluoromethyl)-2H-chromen-2-one (aomc)

The Schiff base was synthesized from the condensation reaction between 7-amino-4-(trifluoromethyl)coumarin (0.2684 g; 1.171 mmol) and 2-amino-3-formylchromone (0.2216 g; 1.171 mmol) in methanol (20 cm^3) which was heated under reflux for 3 h. The resultant yellow solution was allowed to cool to room temperature before the light yellow precipitate was filtered and washed using cold methanol and petroleum ether. Yield = 50%; Melting point: 239.9–244.8 $^\circ\text{C}$; Infrared ($\nu_{\text{max}}/\text{cm}^{-1}$): $\nu(\text{N}-\text{H})$ 3242, 3093 (br), $\nu(\text{C}=\text{O})$ 1679 (s), $\nu(\text{C}=\text{N})$ 1610 (s), $\nu(\text{C}-\text{O}-\text{C})$ 1334 (s); ^1H NMR (d_6 -DMSO/298 K/ppm): 10.09 (s, 1H, H11), 9.59 (s, 2H, NH_2),

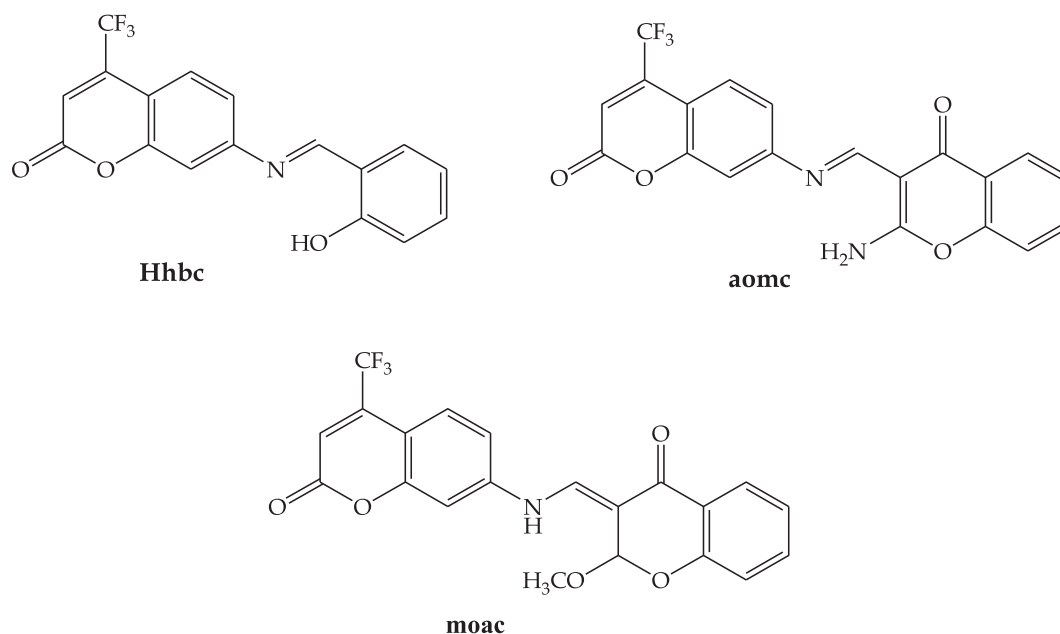


Fig. 1. Structures of the coumarin free-ligands considered within this study.

8.05–8.01 (dd, $J = 7.7$ Hz, $J = 1.7$ Hz, 1H, *H15*), 7.76–7.70 (t, $J = 1.5$ Hz, $J = 1.1$ Hz, 3H, *H17*), 7.48–7.33 (m, 3H, *H8*, *H16*, *H18*), 6.68–6.64 (dd, $J = 8.8$ Hz, $J = 2.2$ Hz, 1H, *H9*), 6.53–6.50 (d, $J = 2.2$ Hz, 1H, *H6*), 6.43 (s, 1H, *H3*); ^{13}C NMR (d^6 -DMSO/295 K/ppm): 188.42 (C13), 175.58 (C20), 165.96 (C4), 159.86 (C19), 157.05 (C2), 154.57 (C11), 153.60 (C5), 134.59 (C7), 126.22 (C9), 126.20 (C14), 125.83 (C16), 125.70 (C1), 122.70 (C17), 117.34 (C15), 112.69 (C18), 107.92 (C10), 107.86 (C8), 102.23 (C6), 99.46 (C3), 99.14 (C12); UV-Vis (Methanol, λ_{max} (ϵ , $\text{M}^{-1} \text{cm}^{-1}$): 377 nm (1361), 292 nm (1297), 264 nm (1785), 234 nm (2698); TOF-MS (m/z): Calcd: 400.0671, Found: 400.0753 $[\text{M}]^+$, 401.0750 $[\text{M}+\text{H}]^+$, 402.0785 $[\text{M}+2\text{H}]^+$.

2.2.3. 7-(((2-Methoxy-4-oxochroman-3-yl)methylene)amino)-4-(trifluoromethyl)-2H-chromen-2-one (moac)

An equimolar ratio of 7-amino-4-(trifluoromethyl)coumarin (0.3300 g; 1.44 mmol) and 3-formylchromone (0.2508 g; 1.44 mmol) in methanol (20 cm^3) was heated under reflux for 3 h. The resultant yellow solution was allowed to cool to room temperature before the yellow precipitate was filtered, washed with cold methanol and petroleum ether. Yield = 92%; Melting point: 174.1–175.9 $^{\circ}\text{C}$; Infrared ($\nu_{\text{max}}/\text{cm}^{-1}$): $\nu(\text{O}-\text{CH}_3)$ 3092 (s), $\nu(\text{N}-\text{H})$ 2933 (br), $\nu(\text{C}=\text{O})$ 1725 (s), $\nu(\text{C}-\text{O}-\text{C})$ 1268 (s), $\nu(\text{C}-\text{N})$ 1130 (s); ^1H NMR (d^6 -DMSO/298 K/ppm): 11.79–11.70 (d, $J = 12.3$ Hz, 1H, *NH*), 8.24–8.18 (d, $J = 12.3$ Hz, 1H, *H15*), 7.88–7.84 (dd, $J = 1.7$ Hz, $J = 7.7$ Hz, 1H, *H17*), 7.69–7.65 (m, 2H, *H16*, *H18*), 7.60–7.55 (m, 1H, *H11*), 7.49–7.45 (dd, $J = 2.3$ Hz, $J = 8.8$ Hz, 1H, *H9*), 7.19–7.09 (m, 2H, *H6*, *H8*), 6.90 (s, 1H, *H3*), 5.85 (s, 1H, *H20*), 3.41 (s, 3H, *H21*); ^{13}C NMR (d^6 -DMSO/295 K/ppm): 181.22 (C13), 158.98 (C19), 156.17 (C4), 155.92 (C2), 144.65 (C5), 143.86 (C7), 139.78 (C11), 139.46 (C17), 135.50 (C15), 126.48 (C9), 126.22 (C1), 122.86 (C16), 122.62 (C14), 118.67 (C12), 114.77 (C18), 109.02 (C8), 106.22 (C3), 104.23 (C10), 101.58 (C6), 55.48 (C20), 49.07 (C21); UV-Vis (Methanol, λ_{max} (ϵ , $\text{M}^{-1} \text{cm}^{-1}$): 404 nm (11660), 325 nm (sh, 1335), 270 nm (sh, 1701), 240 nm (2949); TOF-MS (m/z): Calcd: 417.0824, Found: 386.0936 $[\text{M}-\text{OCH}_3]^+$, 387.0983 $[\text{M}-\text{OCH}_3 + \text{H}]^+$.

2.3. Synthesis of metal complexes

2.3.1. *trans*-[ReOBr₂(PPh₃)₃](hbc) (1)

Complex **1** was isolated from the reaction of Hhbc (0.034 g; 1.035 mmol) and *trans*-[ReOBr₃(PPh₃)₂] (0.100 g; 1.035 mmol) in toluene (20 cm^3) at reflux for 4 h. The resultant dark green solution was allowed to cool to room temperature and was filtered. Slow evaporation of the mother liquor produced green needle crystals. Yield: 48%; Melting point: 236–240 $^{\circ}\text{C}$; Conductivity (EtOH, 10^{-3} M) = 20.45 $\text{ohm}^{-1} \text{cm}^2 \text{mol}^{-1}$; Infrared ($\nu_{\text{max}}/\text{cm}^{-1}$): $\nu(\text{C}=\text{O})$ 1750 (s), $\nu(\text{C}=\text{N})$ 1595 (s), $\nu(\text{C}-\text{O}-\text{C})$ 1181 (s), $\nu(\text{Re}=\text{O})$ 973 (s); ^1H NMR (d^6 -DMSO/298 K/ppm): 8.02–7.89 (m, 2H, *H13*, *H15*), 7.85–7.73 (m, 3H, *H6*, *H8*, *H9*), 7.69–7.53 (m, 16H, *PPh3*, *H11*), 7.38–7.10 (m, 3H, *H3*, *H14*, *H16*); ^{13}C NMR (d^6 -DMSO/295 K/ppm): 161.19 (C11), 158.73 (C4), 158.55 (C17), 157.03 (C2), 154.50 (C7), 153.84 (C5), 139.24 (C15), 139.09 (C13), 136.88 (PPh₃), 134.60 (PPh₃), 134.52 (PPh₃), 133.81 (PPh₃), 132.81 (PPh₃), 132.51 (PPh₃), 132.49 (PPh₃), 132.13 (PPh₃), 131.99 (PPh₃), 131.91 (PPh₃), 130.52 (PPh₃), 129.75 (PPh₃), 129.36 (PPh₃), 129.27 (PPh₃), 129.21 (PPh₃), 129.18 (PPh₃), 128.67 (PPh₃), 125.79 (C9), 122.79 (C1), 121.11 (C14), 120.57 (C10), 119.96 (C8), 118.17 (C12), 117.70 (C16), 112.85 (C6), 112.73 (C3); UV-Vis (Methanol, λ_{max} (ϵ , $\text{M}^{-1} \text{cm}^{-1}$): 589 nm (sh, 73), 489 nm (sh, 180), 371 nm (5642), 259 nm (9148); Molecular mass (m/z): Calcd: 956.5533, Found: 876.038 $[\text{M}-\text{Br}]^+$, 878.043 $[\text{M}-\text{Br} + 2\text{H}]^+$.

2.3.2. *fac*-[Re(CO)₃Cl(aomc)] (2)

An equimolar reaction mixture of [Re(CO)₅Cl] (1.000 g; 2.764 mmol) and ligand aomc (0.110 g; 2.764 mmol) in toluene (20 cm^3) was heated under nitrogen to reflux for 6 h. From the resulting orange solution, a yellow precipitate was obtained via gravity filtration and washed with diethyl ether. Yield: 68%; Melting point: 263–266 $^{\circ}\text{C}$; Conductivity (EtOH, 10^{-3} M) = 3.92 $\text{ohm}^{-1} \text{cm}^2 \text{mol}^{-1}$; Infrared ($\nu_{\text{max}}/\text{cm}^{-1}$): $\nu(\text{N}-\text{H})$ 3312, 3128 (br, m), $\nu(\text{C}=\text{O})_{\text{fac}}$ 2023, 1902 (vs), $\nu(\text{C}=\text{O})_{\text{coumarin}}$ 1747 (s), $\nu(\text{C}=\text{O})_{\text{chromone}}$ 1646 (s), $\nu(\text{C}=\text{N})$ 1605 (s), $\nu(\text{C}-\text{O}-\text{C})$ 1339 (s); ^1H NMR (d^6 -DMSO/298 K/ppm): 10.13–9.88 (d, 2H, *NH2*), 8.59 (s, 1H, *H11*), 8.13–8.09 (dd, $J = 8.1$ Hz, $J = 1.5$ Hz, 1H, *H9*), 7.93–7.86 (m, 2H, *H6*, *H8*), 7.62–7.55 (m, 2H, *H15*, *H17*), 7.50–7.44 (m, 2H, *H1*, *H18*), 7.10 (s, 1H, *H16*); ^{13}C NMR (d^6 -DMSO/295 K/ppm): 188.43 (C13), 171.47 (C20), 168.11 (C4), 159.90 (C=O)_{fac}, 159.32 (C=O)_{fac}, 158.64 (C=O)_{fac}, 154.19 (C19), 151.94 (C2), 135.94 (C11), 134.63 (C5), 129.36 (C7), 128.66 (C9), 126.96 (C14), 126.45 (C16), 125.71 (C1), 121.44 (C17), 119.59 (C15), 117.37 (C18), 117.31 (C10), 112.32 (C8), 111.99 (C6), 99.13 (C3), 97.90 (C12); UV-Vis (Methanol, λ_{max} (ϵ , $\text{M}^{-1} \text{cm}^{-1}$): 263 nm (19041), 291 nm (17658), 333 nm (sh, 12608), 392 nm (sh, 6560); Molecular mass (m/z): Calcd: 705.9764, Found: 702.9614 $[\text{M}-2\text{H}]^-$, 704.9639 $[\text{M}-\text{H}]^-$, 706.9764 $[\text{M} + \text{H}]^-$.

2.3.3. *fac*-[Re(CO)₃Cl(moac)] (3)

A solution of [Re(CO)₅Cl] (0.100 g; 2.765 mmol) and moac (0.106 g; 2.765 mmol) in toluene (20 cm^3) was heated to reflux under nitrogen for 6 h. The yellow solution was cooled to room temperature and the yellow precipitate was filtered, washed with diethyl ether. Yield: 44%; Melting point: 270–273 $^{\circ}\text{C}$; Conductivity (EtOH, 10^{-3} M) = 5.26 $\text{ohm}^{-1} \text{cm}^2 \text{mol}^{-1}$; Infrared ($\nu_{\text{max}}/\text{cm}^{-1}$): $\nu(\text{O}-\text{CH}_3)$ 3190 (s), $\nu(\text{N}-\text{H})$ 2943 (s), $\nu(\text{C}=\text{O})_{\text{fac}}$ 2020, 1906, 1887 (s), $\nu(\text{C}=\text{O})_{\text{coumarin}}$ 1756 (s), $\nu(\text{C}=\text{O})_{\text{chromone}}$ 1638 (s), $\nu(\text{C}-\text{O}-\text{C})$ 1253 (s), $\nu(\text{C}-\text{N})$ 1144 (s); ^1H NMR (d^6 -DMSO/298 K/ppm): 9.52 (s, 1H, *H3*), 8.79 (s, 1H, *H11*), 8.40–8.35 (d, 1H, *H9*), 8.21–8.15 (t, 1H, *H18*), 8.08–8.04 (d, 1H, *H16*), 8.00–7.95 (d, 1H, *H15*), 7.86–7.81 (t, 1H, *H17*), 7.52–7.46 (m, 2H, *H6*, *H8*), 7.14 (s, 1H, *H20*), 3.43 (s, 6H, *OCH3*, *NH*, *H20*); UV-Vis (Methanol, λ_{max} (ϵ , $\text{M}^{-1} \text{cm}^{-1}$): 261 nm (15581), 298 nm (br, 16449), 331 nm (br, 16885), 415 nm (16942); Molecular mass (m/z): Calcd: 721.9839, Found: 707.9677 $[\text{M}-\text{CH}_3]^-$, 705.9655 $[\text{M}-\text{CH}_3-2\text{H}]^-$.

2.4. DNA binding studies

The DNA binding properties of **2** and **3** were investigated via the titration of the metal complexes using Calf-Thymus (CT)-DNA prepared in aqueous PBS (pH 7.4). The study was conducted at 25 $^{\circ}\text{C}$ using a temperature-controlled system. CT-DNA stock solutions were prepared and stored as per the instructions by Sigma-Aldrich. The CT-DNA solution afforded a UV absorbance ratio at 260 and 280 nm of 1.8:1 indicating the DNA was sufficiently free of bound proteins [17]. In addition, using the molar absorptivity per nuclide of DNA ($\epsilon = 6600 \text{M}^{-1} \text{cm}^{-1}$) and the UV absorption at 260 nm, the concentration of the DNA stock solution was calculated. The respective metal complex and CT-DNA solutions were incubated for 24 h at 25 $^{\circ}\text{C}$ prior to any UV-Vis measurements. Furthermore, the UV-Vis spectra of the metal complexes (in methanol) was attained with varying nucleotide concentrations. The intrinsic binding constant (K_b) of metal complexes **2** and **3** were obtained using the Wolfe-Shimmer equation (Eq. (A)):

$$[\text{DNA}]/(\epsilon_a - \epsilon_f) = [\text{DNA}]/(\epsilon_b - \epsilon_f) + 1/K_b(\epsilon_b - \epsilon_f) \quad (\text{A})$$

In the equation, [DNA] is the concentration of DNA in base pairs, ϵ_a is the extinction coefficient of the absorption band at the given [DNA] ($A_{\text{obs}}/[\text{complex}]$), ϵ_f is the extinction coefficient of the complex free in solution, and ϵ_b is the extinction coefficient of the com-

Table 1
Crystal data and structure refinement data.

	Hhbc	moac	1
Chemical formula	C ₁₇ H ₁₀ F ₃ NO ₃	C ₂₁ H ₁₄ F ₃ NO ₅	C ₄₂ H ₃₂ Br ₂ F ₃ NO ₄ PRE
Formula weight	332.26	417.33	1048.68
Crystal system	monoclinic	triclinic	monoclinic
Space group	<i>P</i> 2 ₁ / <i>n</i>	<i>P</i> $\bar{1}$	<i>P</i> 2 ₁ / <i>n</i>
<i>T</i> (K)	100(2)	100(2)	100(2)
Unit cell dimension			
<i>a</i> (Å)	9.8163(7)	8.2277(6)	19.463(2)
<i>b</i> (Å)	5.4034(3)	9.6581(7)	9.2113(11)
<i>c</i> (Å)	26.2875(19)	12.2234(8)	21.033(3)
α (°)	90	92.902(4)	90
β (°)	90.436(4)	96.587(4)	97.030(2)
γ (°)	90	93.859(4)	90
Crystal size (mm)	0.60 × 0.11 × 0.04	0.17 × 0.12 × 0.09	0.21 × 0.03 × 0.02
<i>V</i> (Å ³)	1394.29(16)	961.05(12)	3742.5(8)
<i>Z</i>	4	2	4
<i>D</i> _{calc.} (Mg m ⁻³)	1.588	1.442	1.861
Absorption coefficient (mm ⁻¹)	0.136	0.122	5.490
<i>F</i> (000)	680	428	2040
θ range for data collection (°)	1.5, 27.1	1.7, 27.1	1.32, 26.01
Index ranges	−12 ≤ <i>h</i> ≤ 12 −4 ≤ <i>k</i> ≤ 6 −32 ≤ <i>l</i> ≤ 33	−10 ≤ <i>h</i> ≤ 10 −12 ≤ <i>k</i> ≤ 12 0 ≤ <i>l</i> ≤ 15	−24 ≤ <i>h</i> ≤ 23 −6 ≤ <i>k</i> ≤ 11 −25 ≤ <i>l</i> ≤ 25
Reflections measured	12 651	4151	25 931
Observed reflections [<i>I</i> > 2σ(<i>I</i>)]	2358	3091	5881
Independent reflections	3056	4151	7174
Data/restraints/parameters	3056, 0, 221	4151, 0, 272	7174, 0, 488
Goodness-of-fit (GOF) on <i>F</i> ²	1.04	1.060	1.01
Observed <i>R</i> , <i>wR</i> ²	0.042, 0.105	0.055, 0.161	0.026, 0.049
<i>R</i> _{int}	0.029	0.033	0.038

Table 2
Selected bond lengths (Å) and bond angles (°) of 1.

	1	
	Computed	Experimental
Bond length (Å)		
Re–N	2.115	2.157(3)
Re–Br1	2.570	2.547(5)
Re–Br2	2.574	2.564(5)
Re–O3	1.979	1.937(2)
Re–O4	1.678	1.686(2)
Re–P	2.499	2.472(1)
Bond angle (°)		
Br1–Re1–P1	90.1	87.5(2)
Br1–Re1–Br2	168.9	170.1(1)
Br1–Re1–O3	86.9	86.7(7)
Br1–Re1–O4	95.8	97.0(8)
Br1–Re1–N1	88.3	90.5(8)
P1–Re1–Br2	96.6	97.5(2)
P1–Re1–O3	84.7	89.6(7)
P1–Re1–O4	90.9	94.2(8)
P1–Re1–N1	167.8	171.2(8)
Br2–Re1–O3	84.9	84.7(7)
Br2–Re1–O4	92.9	91.3(8)
Br2–Re1–N1	83.3	83.3(8)
O3–Re1–O4	174.9	174.8(1)
O3–Re1–N1	83.1	81.7(1)
O4–Re1–N1	101.3	94.6(1)

plex when fully bound to DNA. A plot of [DNA]/($\epsilon_a - \epsilon_f$) versus [DNA], gave a slope of $1/(\epsilon_a - \epsilon_f)$ and *y*-intercept equal to $1/K_b(\epsilon_b - \epsilon_f)$. Using the slope to intercept ratio the intrinsic binding constant, *K_b*, is obtained.

2.5. X-ray diffraction

The X-ray data for metal complex **1** and free-ligands, Hhbc and moac were recorded on a Bruker Apex Duo diffractometer

Table 3
Selected bond lengths (Å) and bond angles (°) for Hhbc and moac.

Hhbc		moac	
C7–N1	1.421(2)	C7–N1	1.398(3)
N1–C11	1.287(2)	N1–C11	1.354(3)
C11–C12	1.451(2)	C11–C12	1.364(3)
C12–C17	1.409(2)	C12–C20	1.500(3)
C4–O2	1.368(2)	C4–O2	1.378(3)
C5–O2	1.387(2)	C5–O2	1.381(2)
–	–	C19–O4	1.379(3)
–	–	C20–O9	1.433(3)
C7–N1–C11	120.5(1)	C7–N1–C11	125.4(2)
N1–C11–C12	121.7(2)	N1–C11–C12	123.8(2)
C11–C12–C17	121.8(1)	C11–C12–C20	117.5(2)
C11–C12–C13	119.1(1)	C11–C12–C13	123.7(2)

equipped with an Oxford Instruments Cryojet, operating at 100 (2) K, and an Incoatec microsource, operating at 30 W power. In all three cases the data were collected with Mo *K*α ($\lambda = 0.71073$ Å) radiation at a crystal-to-detector distance of 50 mm. The data collections were performed using omega and phi scans with exposures taken at 30 W and 0.50° frame widths using APEX2 [18]. The data were reduced with the programme SAINT [18] using outlier rejection, scan speed scaling, as well as standard Lorentz and polarization correction factors. A SADABS semi-empirical multi-scan absorption correction was applied to the data [18]. Direct methods, SHELXS-97 [19] and WinGX [20] were used to solve all three structures. All non-hydrogen atoms were located in the difference density map and refined anisotropically with SHELXL-97 [19]. All hydrogen atoms were included as idealized contributors in the least squares process. Their positions were calculated using a standard riding model with C–H_{aromatic} distances of 0.95 Å and $U_{iso} = 1.2 U_{eq}$ and C–H_{methylene} distances of 0.99 Å and $U_{iso} = 1.2 U_{eq}$. Crystal and structure refinement data are given in Table 1 and selected bond lengths and bond angles are given in Tables 2 and 3. Platon SQUEEZE was used to remove disordered solvent

molecules from the crystal lattice of moac [21]. The squeeze process left solvent accessible voids of 71 Å³. The solvent was a methanol molecule disordered over a position of too high symmetry for the molecule.

2.6. Computational studies

The coumarin free-ligands (*viz.* Hhbc, aomc and moac) and the metal complexes **1–3** were optimised using the DFT method with the PBE1PBE functional in conjunction with the 6-31G basis set for hydrogen and carbon atoms, the 6-31+G(d) basis set for nitrogen, oxygen, chlorine and phosphorus atoms as well as the effective core pseudopotential LANL2DZ basis set for rhenium atom. The use of the PBE1PBE functional and the aforementioned basis sets have been justified in literature for rhenium-containing complexes [22]. Full optimisation, without any symmetry restrictions, was adopted in the gas phase. The X-ray structures were used for Hhbc, moac and metal complex **1** as starting conformers. As the X-ray structures for **2** and **3** are not available, the *facial* tricarbonylrhenium(I) configuration for each metal complex was considered. All the free-ligands and their metal complexes were optimised with a multiplicity of 1. Frequency computations of their optimised geometries were performed to ensure that all conformers are true local minima. Uncorrected infrared vibrational frequencies of these compounds were also reported in the gas phase. In order to mimic the experimental conditions, the free-ligands and the metal complexes **1–3** were optimised in dimethyl sulfoxide (DMSO) and methanol as solvents. These solvent computations were carried out using the polarizable continuum model as developed by Tomasi's group [23] in the framework of self-consistent reaction field. In addition, the optimized structures in DMSO were used for computing the chemical shifts of the metal complexes with the Gauge-Including Atomic Orbital method [24] using shielding of TMS computed at the same theoretical level and basis set. TD-DFT computations were also performed using the optimised structures in methanol to obtain the electronic spectra. GAUSSIAN 09 program [25] was used for all the computations by means of the resources provided by Gridchem [26].

Molecular docking simulations were carried out using the optimized structures of **2** and **3** and the programme Patchdock Beta

version 1.3. Molecular interactions were refined using Firedock [27] and visualizations were adapted through YASARA View [28]. The B-DNA structure (LOX) (PDB ID: 1F8N) was obtained from the Protein Data Bank and all water molecules were removed prior to the docking procedure.

3. Results and discussion

3.1. Synthesis, spectral characterization and computational studies

The diamagnetic rhenium(V) and -(I) complexes **1–3** were isolated from the 1:1 M coordination reactions of the coumarin free-ligands (*viz.* Hhbc; aomc and moac) with *trans*-[ReOBr₃(PPh₃)₂] and [Re(CO)₅Cl], see Schemes 1–6 in the supporting information document. These bidentate coumarin chelators coordinate through their mono anionic N_{imino}O_{phenolate} (for **1**) and neutral N_{imino}O_{ketonic} donor sets (for **2** and **3**). Complex **1** is soluble in most polar solvents while the rhenium(I) compounds are partially soluble in halogenated solvents and soluble in hot aprotic solvents and methanol. The rhenium complexes are stable in the solid-state and for months in methanol. With the exception of complex **3** being progressively unstable over three to four hours in dimethylsulphoxide, the other rhenium complexes are stable in this solvent for days.

The distinctive features of the IR spectra of the metal complexes are the characteristic intense vibrations associated with the [Re^{VO}]³⁺ (for **1**) and *fac*-[Re(CO)₃]⁺ cores (for **2** and **3**). The analogous stretches obtained theoretically are found at 1060 cm⁻¹ (for **1**) and between 1985 and 2104 cm⁻¹ (2104, 2023, 1985 cm⁻¹ for **2** and 2114, 2028, 1999 cm⁻¹ for **3**) within their respective simulated IR spectra, see Figs. S15, S21 and S26. Interestingly, the theoretical assignment of the vibrational modes show that the ketonic groups of the coordinated chromone moieties (1636 cm⁻¹ for **2** and 1653 cm⁻¹ for **3**) vibrate at lower frequencies compared to the uncoordinated coumarin moieties (1824 cm⁻¹ for **2** and 1826 cm⁻¹ for **3**) for the *facial* tricarbonylrhenium(I) compounds. Therefore, their ketonic coumarin IR stretches in the experimental spectra are found at 1747 (for **2**) and 1756 cm⁻¹ (for **3**) while the ketonic chromone IR stretches are found at 1646 (for **2**) and 1638 cm⁻¹ (for **3**).

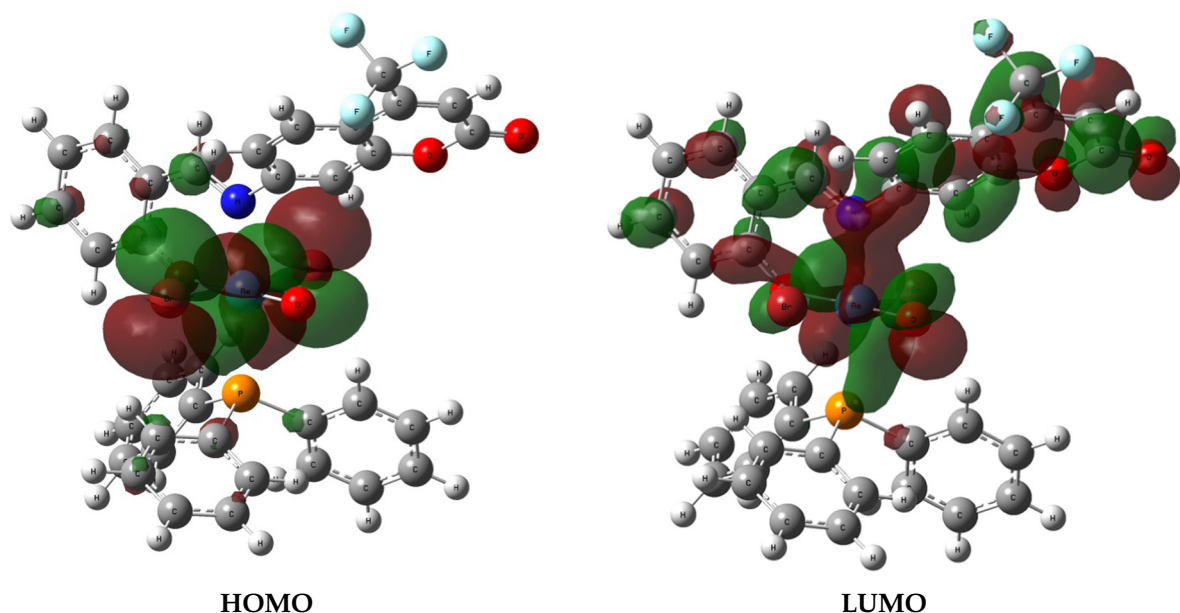


Fig. 2. HOMO and LUMO surfaces of metal complex **1** in methanol.

The absence of the $\nu(\text{C}=\text{N})$ of **3** in its experimental spectrum is also evident in the simulated spectrum of **3** while an amine vibration is observed at 1144 cm^{-1} and 1149 cm^{-1} in its experimental and simulated IR spectra, respectively. Computationally, the symmetric CH stretching of the methoxy group vibrates strongly at 3065 cm^{-1}

and its experimental vibrational band occur as a medium intense as well as broad vibrational band.

The proton spectrum of **1** is dominated by a multiplet ascribed to the triphenylphosphine co-ligand and the imino protons' signals. The remaining signals of the aromatic moieties appear in

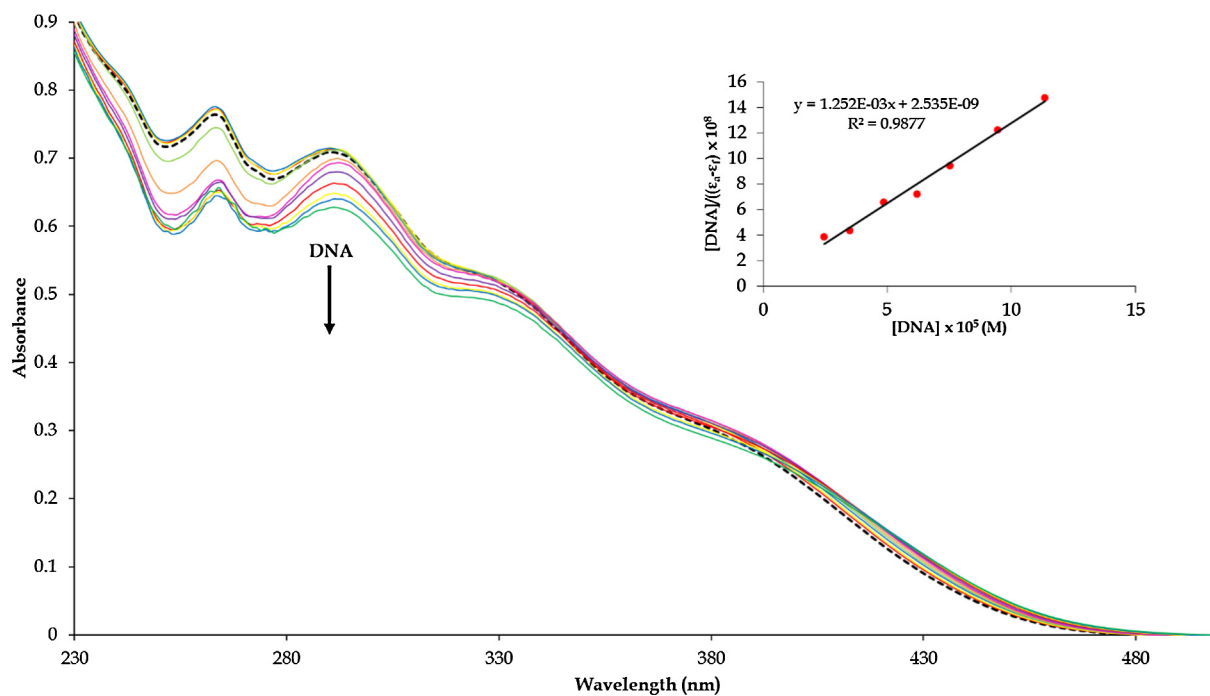


Fig. 3. UV-Vis spectral profile of **2** attained from the titration of **2** against progressive additions of CT-DNA. The arrow indicates the decreasing intensity of the intra-ligand electronic transition at 291 nm. The inset shows the plot of $[\text{DNA}]/(\epsilon_a - \epsilon_f) \times 10^8$ vs $[\text{DNA}] \times 10^5$.

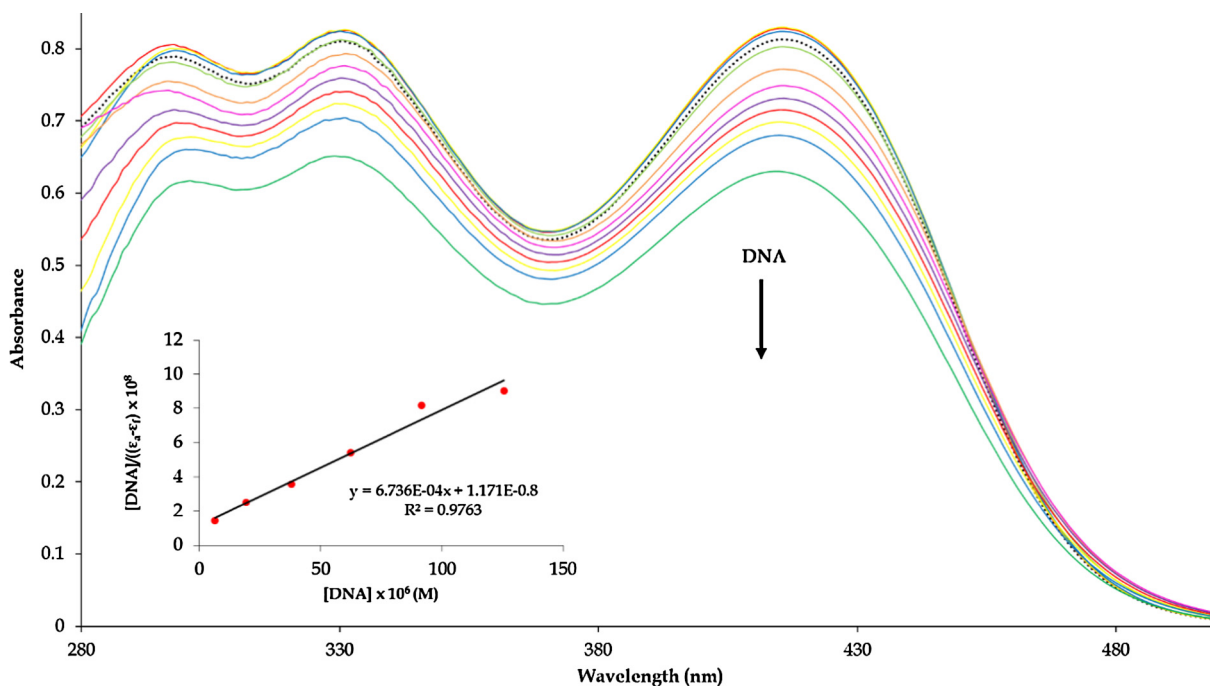


Fig. 4. UV-Vis spectral profile of **3** attained from the titration of **3** against progressive additions of CT-DNA. The arrow indicates the decreasing intensity of the intra-ligand electronic transition at 415 nm. The inset shows the plot of $[\text{DNA}]/(\epsilon_a - \epsilon_f) \times 10^8$ vs $[\text{DNA}] \times 10^6$.

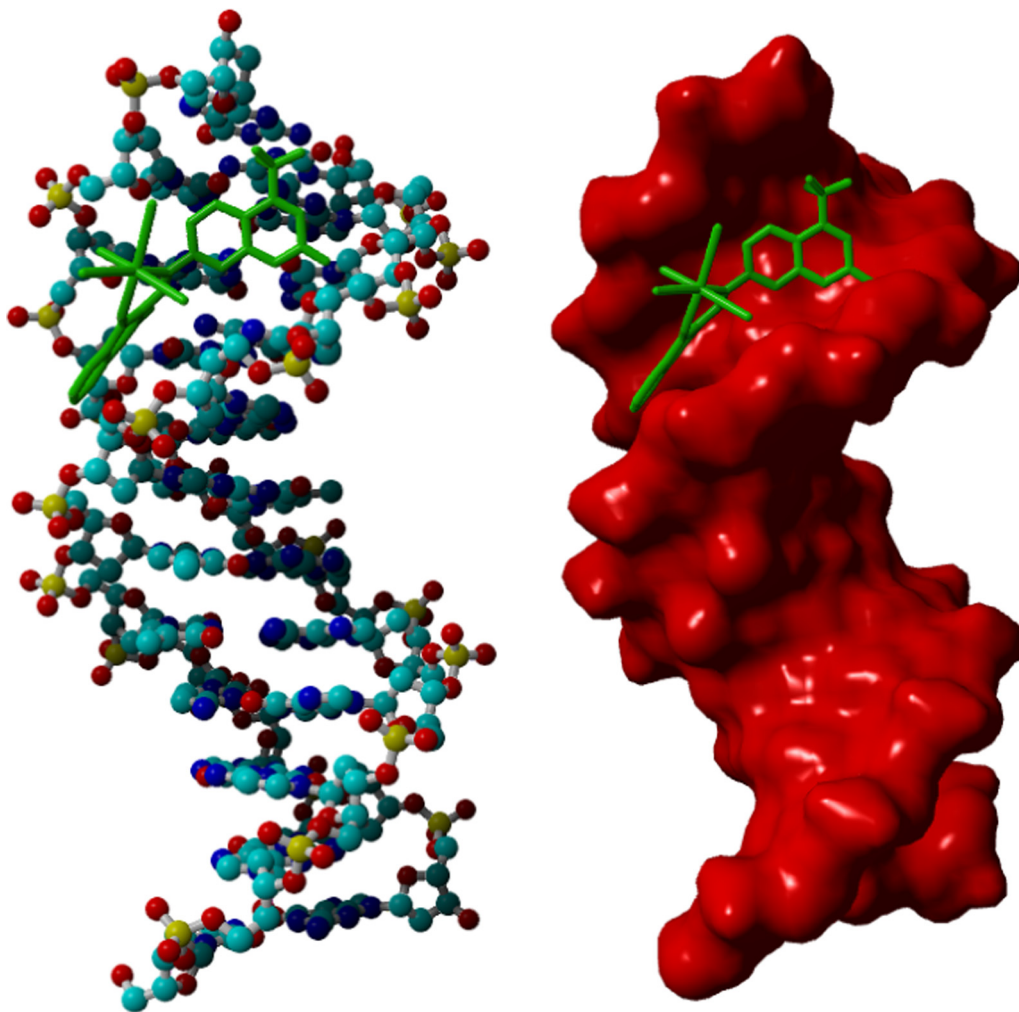


Fig. 5. Docked position of **2** bound to a minor groove of B-DNA: (A) shows DNA in ball and stick view whereas (B) shows the molecular surface view of DNA.

the form of three multiplets integrating to 2, 3 and 3 protons, see Fig. S10. The comparative imine and amine C–H signals of **2** (at 8.59 ppm) and **3** (8.79 ppm) resonate at significantly different positions which emphasizes again that moac chelator is an amine, see Figs. S17 and S23. In addition, the predicted NMR spectra of **2** and **3** show individual C–H signals at 8.42 ppm and 8.94 ppm, which are in good agreement with the experimental findings.

The classical covalent attachment of a methoxy group at the 2-position of the chromone moiety in **3** induced resonance of the imino double bond and protonation of the imino nitrogen [29]. Evidently, a broad singlet at 3.43 ppm in the proton spectrum of **3** is accounted to overlapping signals of the methoxy, the amine and water. The signals of the methoxy group of complex **3** were predicted in the range of 3.82–4.46 ppm. Affirmation that the respective chelators did coordinate to the metal centres is given by the disappearance of the hydroxyl signal in the proton spectrum of **1** which was originally found at 12.37 ppm (predicted at 12.50 ppm) in the proton spectrum of its free-ligand, Hhbc. Furthermore, the ^1H NMR signals of the free ligand aomc differ from that of complex **2**, showing a significant up-field shift for the imine proton with the sharp singlet moving from 10.09 ppm (predicted at 8.74 ppm) to 8.59 ppm (predicted at 8.42 ppm). In addition, the proton signals of **2** between 10.13 and 9.88 ppm shows the presence of the amino substituent implying that coordination did occur via the N_{imino} , O_{ketonic} donor set while all the other aomc ligand's signals show a slight up-field shift. No interpretable ^{13}C NMR spec-

trum of **3** could be obtained which ascribed to its instability in deuterated dimethylsulphoxide and this was confirmed by variable temperature proton NMR spectroscopy. In addition, the moderate solubility of complex **3** in deuterated methanol and acetonitrile afford ^{13}C NMR spectra with low signal-to-noise ratios.

The UV–Vis spectra of the metal complexes exhibit several common intra-ligand π – π^* electronic transitions with that of their respective free-ligands, see Figs. S12, S19 and S24. The electronic spectrum of **1** displays an intra-ligand π – π^* transitions present at 259 nm and 371 nm together with a metal to ligand charge transfer (MLCT) band at 489 nm. The simulated absorption spectra based on TD-DFT computations in methanol of metal complex **1** with Hhbc ligand are illustrated in Fig. S13. There is a close similarity between the experimental and simulated spectra whereby the intra-ligand π – π^* transitions are predicted at 256 nm (oscillator strength, $f = 0.1036$) and 331 nm ($f = 0.1221$). The highest occupied molecular orbital (HOMO) and lowest unoccupied molecular orbital (LUMO) are displayed in Fig. 2. The calculated HOMO–LUMO energy gap of metal complex **1** based on optimized geometries in methanol is 3.40 eV. Complex **1** displays a d – d electronic transition band at 589 nm whilst **2** and **3** possess no metal-based electronic transition bands due to rhenium(I) complexes having low spin d^6 electronic configurations. The HOMO–LUMO energy gaps of metal complexes **2** and **3** are 3.72 eV and 3.64 eV, respectively, revealing that the charge transfer takes place from the rhenium atom towards the coumarin chelators.

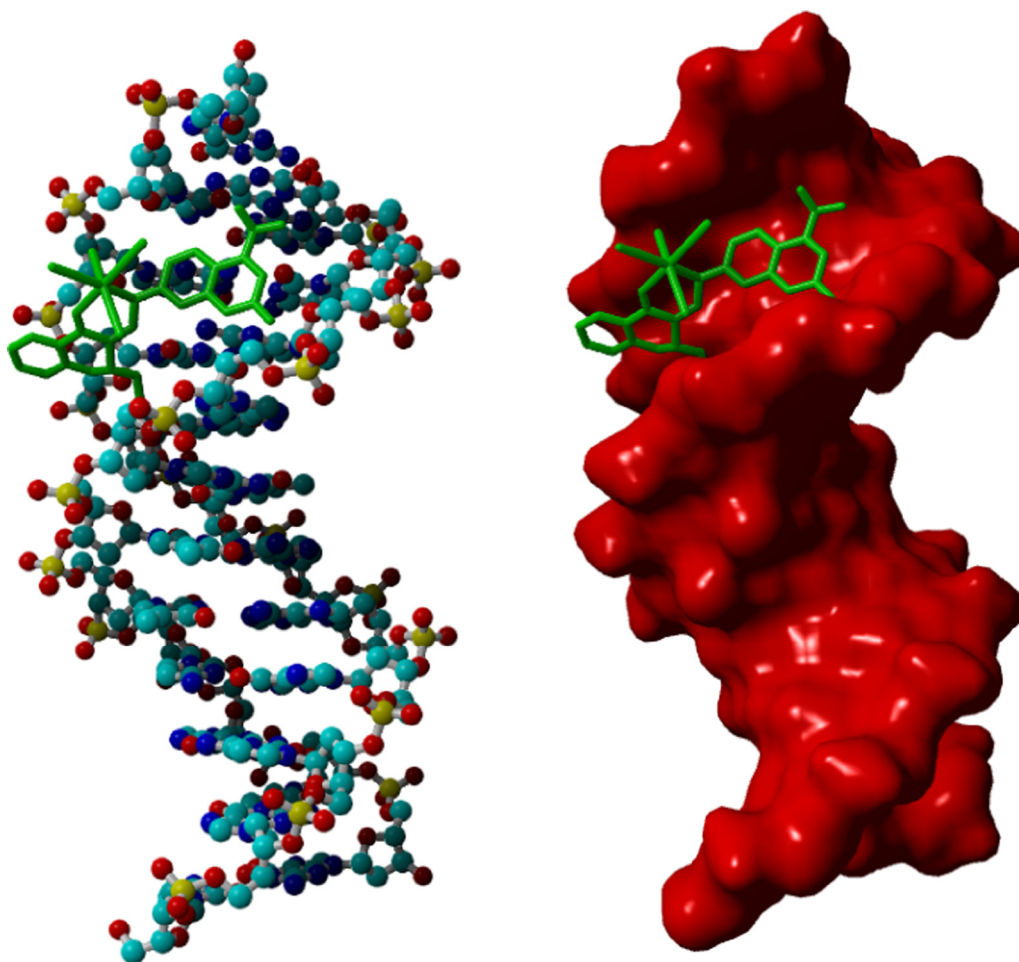


Fig. 6. Docked position of **3** bound to a minor groove of B-DNA: (A) shows DNA in ball and stick view whereas (B) shows the molecular surface view of DNA.

3.1. DNA binding studies

The anticancer activities of many transition metal complexes can be correlated to their DNA interaction capabilities [30]. The interaction of metal complexes and calf thymus DNA is typically monitored using temperature controlled UV–Vis spectroscopy [31,32]. The common DNA binding modes (*viz.* intercalation, groove binding or external electrostatic binding) are typically influenced by the stereo-electronic properties of chelating ligands and steric effects of other co-ligands [33]. Metal complexes which bind to DNA *via* intercalation in progressive decreases of intra-ligand π – π^* electronic transitions or MLCT bands (*i.e.* hypochromism) accompanied by a progressive red shift (*i.e.* bathochromism).

The UV–Vis spectral profiles of **2** and **3** shows decreases of intra-ligand π – π^* electronic transitions at 291 nm (for **2**) and 415 nm (for **3**), see Figs. 3 and 4. The distinctive reductions of these electronic transitions are indicative of hypochromism but no red-shifting of the peak maxima were observed. This UV–Vis spectral changes are synonymous with groove-binding of octahedral rhenium(I) complexes to the DNA double helix rather than DNA intercalation. In fact, the calculated intrinsic binding constants (K_b) for **2** and **3** were estimated to be $4.939 \times 10^5 \text{ M}^{-1}$ and $5.752 \times 10^4 \text{ M}^{-1}$, respectively and compare well with other rhenium(I) groove binding complexes [34,35].

Molecular docking simulations corroborated the experimental DNA binding studies as the optimized conformers of the rhenium (I) compounds both are minor groove binders, see Figs. 5 and 6.

Furthermore, the preferential minor groove binding occurs despite the fact that their respective van der Waals radii (9.484 Å for **2** and 9.415 Å for **3**) suggest that the conformers are too large to fit in the B-DNA structure's minor groove having a diameter of approximately 12 Å from its geometric centre. The comparable optimized structures of **2** and **3** afforded DNA adducts with similar global energies of -51.86 and -54.09 kJ/mol, respectively. In addition, the DNA binding modes of the conformers are reinforced by the following DNA base pair interactions (below 3 Å): G–C, C–G, G–C and T–A for **2**; G–C, C–G, A–T and T–A for **3**. In addition, the chloro co-ligands and coumarin ketonic oxygens for both conformers **2** and **3** show interactions with opposing phosphate backbones of the double stranded DNA.

3.2. X-ray crystallography studies

Four molecules of **1** crystallizes out in the $P2_1/n$ space group along with four toluene molecules of recrystallization. Within the monoclinic unit cell, adjacent molecules of **1** interacts *via* co-planar phenolate moieties of their respective hbc chelators with an inter-planar spacing of 3.812 Å which is outside the distance of 3.5 Å for classical π – π stacking interactions. The rhenium atom of **1** is at the centre of a distorted octahedron induced by the constrained six-membered chelate ring [$\text{N1–Re–O3} = 81.7(1)^\circ$], see Fig. 7. Consequently, non-linear bond angles [$\text{Br1–Re–Br2} = 170.08(2)^\circ$, $\text{O4–Re–O3} = 174.9(1)^\circ$ and $\text{N1–Re–P1} = 171.20(9)^\circ$] are found within the O4Br2O3Br1 basal plane. The optimised ground state

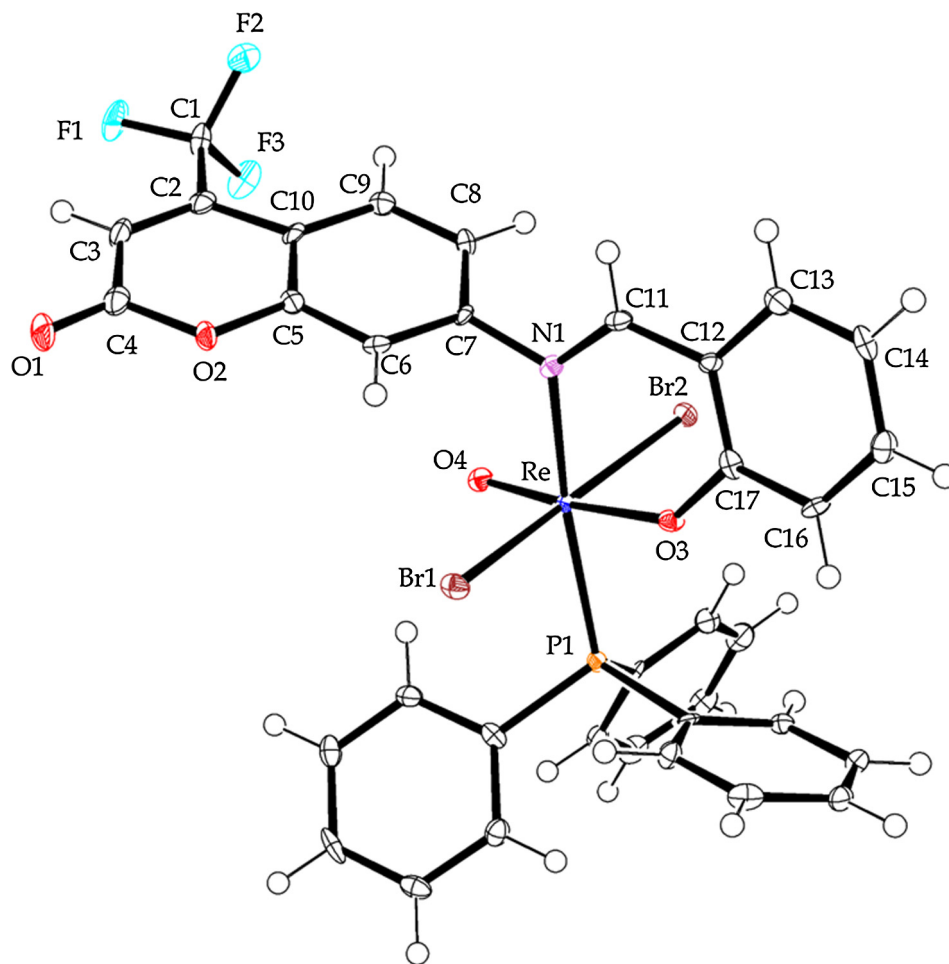


Fig. 7. An ORTEP view of complex **1** showing 50% probability displacement ellipsoids and the atom labelling. The toluene molecule of recrystallization has been omitted for clarity.

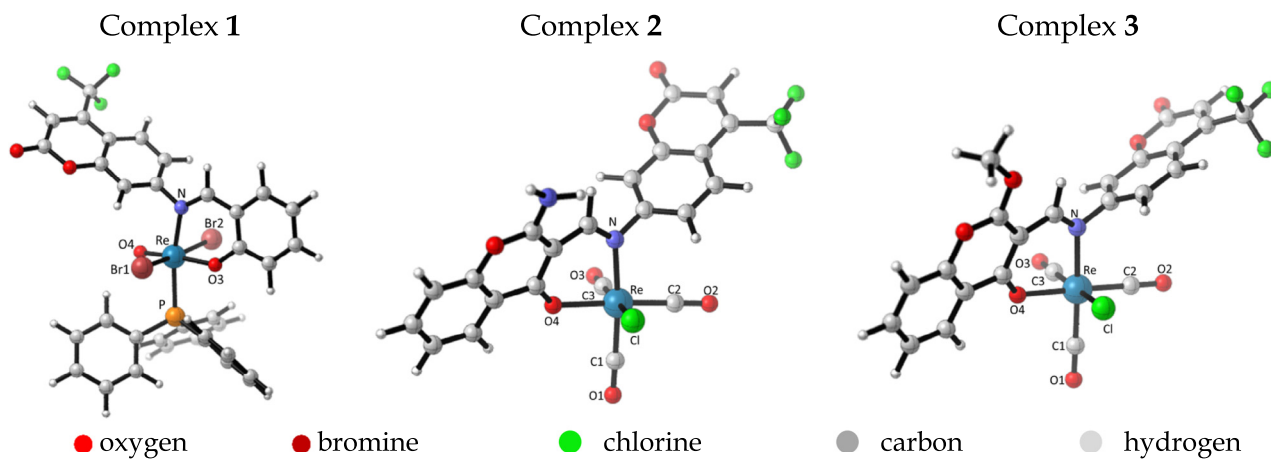


Fig. 8. Optimised geometries of metal complexes **1**, **2** and **3** in the gas phase.

geometries of metal complexes **1**, **2** and **3** in the gas phase are displayed in Fig. 8. Selected bond lengths and angles are gathered in Table 4. These optimised bond lengths and bond angles of metal complex **1** are in good agreement with the experimental data (Tables 2) with root mean square deviations of 0.076 Å and 1.46

Å, respectively. In fact, the simulated bond angles of the chelate rings are 83.1°, 83.4° and 81.5° for metal complexes **1**, **2** and **3**, respectively.

The C11–N1 [1.298(4) Å] bond order of **1** is unequivocally established based on its similarity with Hhbc's imino bond length

Table 4
Selected optimized bond lengths (Å) and bond angles (°) for **2** and **3**.

	2	3
Bond length (Å)	Computed	
Re–Cl	2.476	2.476
Re–N	2.171	2.324
Re–C1	1.924	1.905
Re–C2	1.901	1.906
Re–C3	1.910	1.905
Re–O4	2.177	2.166
C1–O1	1.159	1.160
C2–O2	1.164	1.161
C3–O3	1.167	1.167
Bond angle (°)		
O4–Re–N	83.40	81.50
C1–Re–N	172.38	170.98
C2–Re–O4	176.34	175.62
C3–Re–Cl	174.44	171.92
O1–C1–Re	178.68	178.70
O2–C2–Re	179.17	179.13
O3–C3–Re	179.51	178.63

of 1.287(2) Å while the amine bond of moac [C11–N1 = 1.354(3) Å] are as expected longer than the aforementioned imino bonds, see Figs. 9 and 10. These observations are also made theoretically; the C11–N1 bond length of metal complex **1** is predicted to be 1.302 Å while in the corresponding free ligand, this predicted bond length is 1.295 Å and the C11–N1 bond length of moac is 1.389 Å. The optimised bond lengths and bond angles of Hhbc and moac are found in Tables S1 and S2 in the accompanying supplementary information document and other bond lengths are reported in parentheses so as to assist in the comparison. The consequence of the covalent attachment of a methoxy group to chromone moiety for Hmoac is the resonance of the localized classical C=C bond of C20–C12 [1.499(3) Å, (1.496 Å)] to C12–C11 [1.366(3) Å, (1.368 Å)] whereas the analogous bonds of C20–C12 in **1** [C12–C17 = 1.403(5) Å, (1.418 Å)] and its free-ligand crystal structure, Hhbc [C12–C17 = 1.409(2) Å, (1.421 Å)] are double bonds.

The ketonic bond of the coumarin moiety C4–O1 show similar bond lengths of 1.210(2) Å (1.253 Å) for Hhbc, 1.206(5) Å (1.211 Å) for **1** and 1.206(3) Å (1.211 Å) for moac whilst the ketonic bond

of Hmoac at C13–O3 shows an elongated bond length of 1.247(3) Å (1.253 Å) brought about by intra-ligand hydrogen bonding with the N–H amine. In addition, the ether bonds present in moac of the coumarin moiety [C4–O2 = 1.377(3) Å (1.393 Å) and C5–O2 = 1.381(2) Å (1.370 Å)] and of the chromone moiety [C19–O4 = 1.380(3) Å (1.375 Å) and C20–O4 = 1.433(3) Å (1.437 Å)] show dissimilar bond lengths due to the influence of the methoxy group on C20 whilst Hhbc and **1** both display similar ether bond lengths (e.g. C4–O2 = 1.368(2) Å and C5–O2 = 1.387(2) for Hhbc). These experimental observations also agree well with the optimised bond lengths.

Surprisingly, the rhenium to bromide bonds [Re–Br1 = 2.5467(6) Å (2.570 Å) and Re–Br2 = 2.5638(5) Å (2.574 Å)] are non-equidistant despite their opposing *trans*-influence on each other. The Re–N_{imino} bond [Re–N1 = 2.157(3) Å (2.115 Å)] is well within the range [2.087(9)–2.227(4) Å] found for other oxorhenium(V) Schiff base complexes [36–38]. Furthermore, the Re–O4 [1.686(2) Å (1.678 Å)] and Re–O3 [1.937(2) Å (1.979 Å)] bonds are comparable to other Re–O_{oxo} and Re–O_{phenolate} bonds found within [1.671(8)–1.6967(12) Å] and [1.861(8)–1.99(5) Å], respectively [39–41]. Among these rhenium compounds are *bis*-chloro(*N*-methylsalicylideneimino)oxorhenium(V), [ReOCl₂(Hmap)(PPh₃)] (H₂map = 2-aminobenzylalcohol) and [ReOCl(1b)₂] (1b = 4-nitro-2-(1-methyl-1*H*-pyrazol-3-yl)phenol). In addition, the rhenium to phosphorous bond length in **1** [2.472(1) Å (2.499 Å)] is comparable to those observed in other Re(V) complexes [42–44].

4. Conclusion

Novel rhenium(I) and -(V) complexes with coumarin Schiff bases were synthesized and spectroscopically characterized. DNA binding studies indicated that the *facial* tricarbonyl rhenium(I) compounds are groove-binders which were supported by molecular docking studies. These molecular docking studies illustrated that **2** and **3** are minor groove binders with comparable global energies for their DNA interactions. X-ray crystal structure analysis of **1** revealed that it exhibit a distorted octahedral geometry which largely induced by its constrained N_{imino}–Re–O_{phenolate} bite angle. Density functional theory calculations was also used to complement the experimental data.

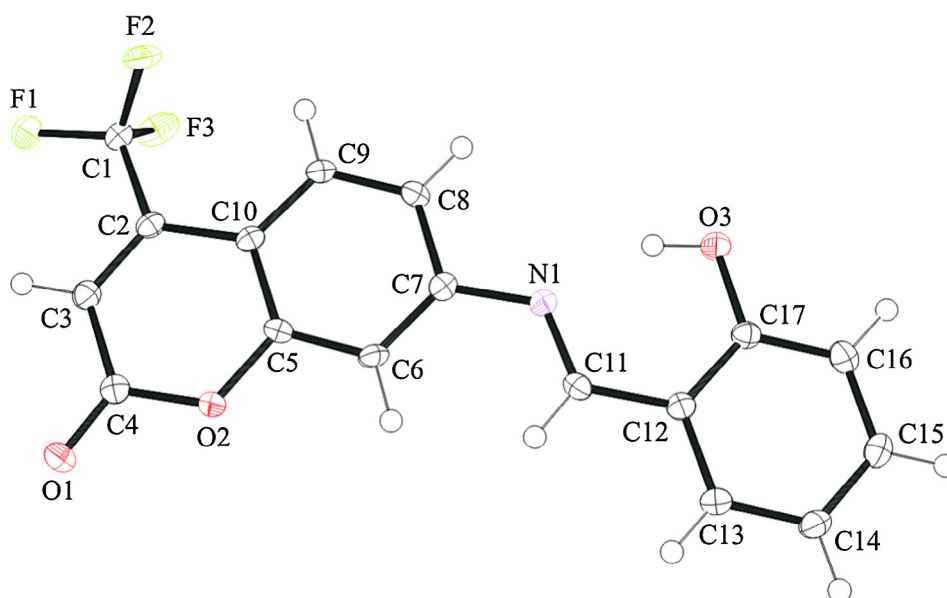


Fig. 9. An ORTEP view of Hhbc showing 50% probability displacement ellipsoids and the atom labelling.

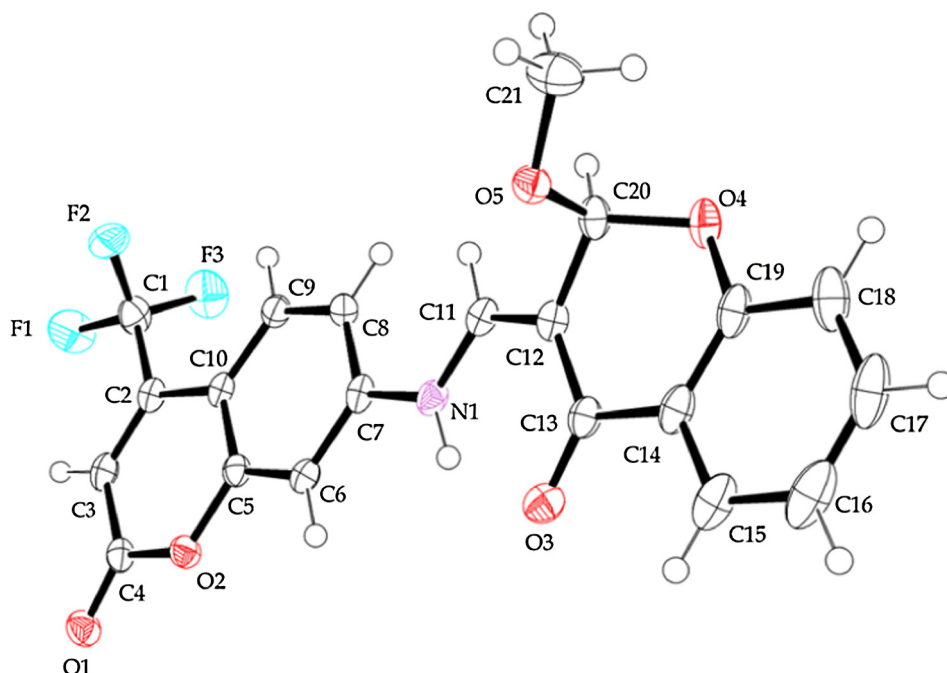


Fig. 10. An ORTEP view of moac showing 50% probability displacement ellipsoids and the atom labelling.

Acknowledgements

We are grateful to the University of KwaZulu-Natal and the National Research Foundation of South Africa for financial support. The authors would also like to thank C.G. Grimmer for the assistance with the interpretation of the NMR data of **3**.

Appendix A. Supplementary data

CCDC 1574752–1574754 contains the supplementary crystallographic data for for metal complex **1** and free-ligands, Hhbc and moac. These data can be obtained free of charge via <http://www.ccdc.cam.ac.uk/conts/retrieving.html>, or from the Cambridge Crystallographic Data Centre, 12 Union Road, Cambridge CB2 1EZ, UK; fax: (+44) 1223-336-033; or e-mail: deposit@ccdc.cam.ac.uk. Supplementary data associated with this article can be found, in the online version, at <https://doi.org/10.1016/j.poly.2018.01.017>.

References

- [1] P.S. Donnelly, The role of coordination chemistry in the development of copper and rhenium radiopharmaceuticals, *Dalton Trans.* 40 (2011) 999.
- [2] M. Bartholomä, J. Valliant, K.P. Maresca, J. Babich, Jon Zubietta, *Single amino acid chelates (SAAC): a strategy for the design of technetium and rhenium radiopharmaceuticals*, *Chem. Commun.* 493 (2009).
- [3] W.A. Volkert, T.J. Hoffman, *Therapeutic Radiopharmaceuticals*, *Chem. Rev.* 99 (1999) 2269.
- [4] A.R. Cowley, J.R. Dilworth, P.S. Donnelly, A mono-diazenide complex from perrhenate: toward a new core for rhenium radiopharmaceuticals, *Inorg. Chem.* 42 (2003) 929.
- [5] A.J. Amoroso, M.P. Coogan, J.E. Dunne, V. Fernandez-Moreira, J.B. Hess, A.J. Hayes, D. Lloyd, C. Millet, S.J.A. Pope, C. Williams, Rhenium fac tricarbonyl bisimine complexes: biologically useful fluorochromones for cell imaging applications, *Chem. Commun.* 3066 (2007).
- [6] L. Huynh, Z. Wang, J. Yang, V. Stoeva, A. Lough, I. Manner, M.A. Winnik, Evaluation of phosphorescent rhenium and iridium complexes in polythiophenylphosphazene films for oxygen sensor applications, *Chem. Mater.* 17 (2005) 4765.
- [7] A. Sachse, N.C. Mosch-Zanetti, G. Lyashenko, J.W. Wielandt, K. Most, J. Magull, F.D. Antonia, A. Pal, R. Herbst-Irmer, Rhenium(V) oxo complexes with acetylacetonate derived schiff bases: structure and catalytic epoxidation, *Inorg. Chem.* 46 (2007) 7129.
- [8] M.B. Ismail, I.N. Booyesen, E. Hosten, M.P. Akerman, Synthesis, characterization and DNA interaction studies of tricarbonyl rhenium(I) compounds containing terpyridine Schiff base chelates, *J. Organomet. Chem.* 833 (2017) 1.
- [9] M. Grazul, E. Budzisz, Biological activity of metal ions complexes of chromones, coumarins and flavones, *Coord. Chem Rev.* 253 (2009) 2588.
- [10] M.A. Musa, J.S. Cooperwood, M.O.F. Khan, A review of coumarin derivatives in pharmacotherapy of breast cancer, *Curr. Med. Chem.* 15 (2008) 2664.
- [11] S.A. Patil, S.N. Unki, A.D. Kulkarni, V.H. Naik, P.S. Badami, Co(II), Ni(II) and Cu(II) complexes with coumarin-8-yl Schiff-bases: Spectroscopic, in vitro antimicrobial, DNA cleavage and fluorescence studies, *Spectrochim. Acta A* 79 (2011) 1128.
- [12] A. Lacy, R. O'Kennedy, Studies on coumarins and coumarin-related compounds to determine their therapeutic role in the treatment of cancer, *Curr. Pharm. Design* 10 (2004) 3797.
- [13] C. Zúñiga, D.P. Oyarzún, R. Martin-Transaco, M. Yáñez-S, A. Telloe, M. Fuentealba, P. Cantero-López, R. Arratia-Pérez, Synthesis, characterization and relativistic DFT studies of fac-Re(CO)₃(isonicotinic acid)₂Cl complex, *Chem. Phys. Lett.* 688 (2017) 66.
- [14] A. Bhattachary, J.P. Naskar, P. Saha, R. Ganguly, B. Saha, S. Tarat Choudhury, S. Chowdhury, A new oxorhenium(V) complex with benzothiazole derived ligand: Relative stability and global chemical reactivity indices, *Inorg. Chim. Acta* 447 (2016) 168.
- [15] G.F. Ciani, G. D'Alfonso, P.F. Romiti, A. Sironi, M. Freni, Rhenium(V) oxide complexes. Crystal and molecular structures of the compounds trans-Re₂O(OR)(PPh₃)₂ (R = Et, Me) and of their hydrolysis derivative ReO₂(PPh₃)₂, *Inorg. Chim. Acta* 72 (1983) 29.
- [16] N.P. Johnson, C.J.L. Lock, G. Wilkinson, Complexes of rhenium(V), *Inorg. Synth.* 145 (1967) 9.
- [17] Deoxyribonucleic acid from calf thymus, product information document, Sigma-Aldrich. <http://www.sigmaaldrich.com/catalog/product/sigma/d4522?lang=en®ion=ZA>, website accessed 18 July 2016.
- [18] Bruker APEX2, SAINT and SADABS. Bruker AXS Inc., Madison, Wisconsin, USA, 2010.
- [19] G.M. Sheldrick, A short history of SHELX, *Acta Cryst.* A64 (2008) 112.
- [20] L.J. Farrugia, WinGX and ORTEP for Windows: an update, *J. Appl. Cryst.* 45 (2012) 849.
- [21] A.L. Spek, Structure validation in chemical crystallography, *Acta Cryst.* D65 (2009) 148.
- [22] K.C. Potgieter, T.I.A. Gerber, R. Betz, L. Rhyman, P. Ramasami, Structural and DFT/TD-DFT investigation of tris(bidentate) complexes of rhenium(III) synthesized from the cis-[ReO₂]⁺ core and benzenethiol derivatives, *Polyhedron* 59 (2013) 91.
- [23] J. Tomasi, B. Mennucci, R. Cammi, Quantum mechanical continuum solvation models, *Chem. Rev.* 105 (2005) 2999.
- [24] K. Wolinski, J.F. Hilton, P. Pulay, Efficient implementation of the gauge-independent atomic orbital method for NMR chemical shift calculations, *J. Am. Chem. Soc.* 112 (1990) 8251.
- [25] M.J. Frisch, G.W. Trucks, H.B. Schlegel, G.E. Scuseria, M.A. Robb, J.R. Cheeseman, G. Scalmani, V. Barone, B. Mennucci, G.A. Petersson, H. Nakatsuji, M. Caricato, X. Li, H.P. Hratchian, A.F. Izmaylov, J. Bloino, G. Zheng, J.L. Sonnenberg, M.

- Hada, M. Ehara, K. Toyota, R. Fukuda, J. Hasegawa, M. Ishida, T. Nakajima, Y. Honda, O. Kitao, H. Nakai, T. Vreven, J.A. Montgomery, J.E. Peralta, F. Ogliaro, M. Bearpark, J.J. Heyd, E. Brothers, K.N. Kudin, V.N. Staroverov, R. Kobayashi, J. Normand, K. Raghavachari, A. Rendell, J.C. Burant, S.S. Iyengar, J. Tomasi, M. Cossi, N. Rega, J.M. Millam, M. Klene, J.E. Knox, J.B. Cross, V. Bakken, C. Adamo, J. Jaramillo, R. Gomperts, R.E. Stratmann, O. Yazyev, A.J. Austin, R. Cammi, C. Pomelli, J.W. Ochterski, R.L. Martin, K. Morokuma, V.G. Zakrzewski, G.A. Voth, P. Salvador, J.J. Dannenberg, S. Dapprich, A.D. Daniels, Ö. Farkas, J.B. Foresman, J.V. Ortiz, J. Cioslowski, D.J. Fox, Gaussian 09 (Revision A.01), 2009, Gaussian Inc., Wallingford CT.
- [26] (a) R. Dooley, K. Milfeld, C. Guiang, S. Pamidighantam, G. Allen, From proposal to production: lessons learned developing the computational chemistry grid cyberinfrastructure, *J. Grid Comput.* 4 (2006) 195;
(b) N. Shen, Y. Fan, S. Pamidighantam, E-science infrastructures for molecular modeling and parametrization, *J. Comput. Sci.* 5 (2014) 576;
(c) This work used the Extreme Science and Engineering Discovery Environment (XSEDE), which is supported by National Science Foundation grant number OCI-1053575.
- [27] (a) D. Duhovny, R. Nussinov, H.J. Wolfson, Efficient unbound docking of rigid molecules, in: Gusfield et al. (ed.), Proceedings of the 2'nd Workshop on Algorithms in Bioinformatics(WABI) Rome, Italy, Lecture Notes in Computer Science, Springer Verlag, 2002, p. 185.;
(b) D. Schneidman-Duhovny, Y. Inbar, R. Nussinov, H.J. Wolfson, PatchDock and SymmDock: servers for rigid and symmetric docking, *Nucl. Acids. Res.* 33 (2005) W363.
- [28] E. Krieger, G. Vriend, New ways to boost molecular dynamics simulations, *J. Comput. Chem.* 36 (2015) 996.
- [29] M. Kalanithi, D. Kodimunthiri, M. Rajaranjan, P. Tharmaraj, Synthesis, characterization and biological activity of some new VO(IV), Co(II), Ni(II), Cu (II) and Zn(II) complexes of chromone based NNO Schiff base derived from 2-aminothiazole, *Spectrochim. Acta A* 82 (2011) 290.
- [30] K.J. Akerman, A.M. Fagenson, V. Cyril, M. Taylor, M.T. Muller, M.P. Akerman, Orde Q. Munro, Gold(III) macrocycles: nucleotide-specific unconventional catalytic inhibitors of human topoisomerase, *J. Am. Chem. Soc.* 136 (2014) 5670.
- [31] L.H. Abdel-Rahman, A.M. Abu-Dief, A.A.H. Abdel-Mawgoud, Development, structural investigation, DNA binding, antimicrobial screening and anticancer activities of two novel quari-dentate VO(II) and Mn(II) mononuclear complexes, *J. King Saud Univ. Sci.* (2017), <https://doi.org/10.1016/j.jksus.2017.05.011>.
- [32] L.H. Abdel-Rahman, R.M. El-Khatib, L.A.E. Nassr, A.M. Abu-Dief, M. Ismael, A.A. Selem, Metal based pharmacologically active agents: Synthesis, structural characterization, molecular modeling, CT-DNA binding studies and in vitro antimicrobial screening of iron(II) bromosalicylidene amino acid chelates, *Spectrochim. Acta A* 7 (2014) 366.
- [33] M. Kaplanis, G. Stamatakis, V.D. Papakonstantinou, M. Paravatou-Petsotas, C.A. Demopoulos, C.A. Mitsopoulou, Re(I) tricarbonyl complex of 1,10-phenanthroline-5,6-dione: DNA binding, cytotoxicity, anti-inflammatory and anti-coagulant effects towards platelet activating factor, *J. Inorg. Biochem.* 135 (2014) 1.
- [34] L.A. Mullice, R.H. Laye, L.P. Harding, N.J. Buurma, S.J.A. Pope, Rhenium complexes of chromophore-appended dipicolylamine ligands: syntheses, spectroscopic properties, DNA binding and X-ray crystal structure, *New. J. Chem.* 32 (2008) 2140.
- [35] R.F. Vitor, I. Correia, M. Videira, F. Marques, A. Paulo, J.C. Pessoa, G. Viola, G.G. Martins, I. Santos, Pyrazolyl-diamine ligands that bear anthracenyl moieties and their rhenium(I) tricarbonyl complexes: synthesis, characterisation and DNA-binding properties, *Chem. Bio. Chem.* 9 (2008) 131.
- [36] F.E. Kuhn, M.U. Rauch, G.M. Lobmaier, G.R.J. Artus, W.A. Herrmann, Rhenium (V) oxo complexes with bidentate schiff bases: structures and catalytic applications, *Chem. Ber.* 130 (1997) 1427.
- [37] S.M. Harben, P.D. Smith, R.L. Beddoes, D. Collison, C.D. Garner, Rhenium and molybdenum oxo-complexes containing ligands related to N-hydroxyiminodipropionic acid, *J. Chem. Soc. Dalton Trans.* 2777 (1997).
- [38] F. Mevellec, A. Roucoux, N. Noiret, H. Patin, Novel six-coordinate oxorhenium (V) '3 + 2' mixed-ligand complexes carrying the SNO/SN donor atom set, *Inorg. Chim. Acta* 332 (2002) 30.
- [39] G. Gilli, M. Sacerdoti, V. Bertolasi, Structure of *chlorobis(N-methylsalicylideneiminato)oxorhenium(V)*, *Acta. Cryst. B*38 (1982) 100.
- [40] G. Bandoli, A. Dolmella, T.I.A. Gerber, D. Mpinda, J. Perils, J.G.H. Du Preez, Complexes of oxorhenium(V) with aromatic 2-amino-alcohols, *J. Coord. Chem.* 55 (2002) 823.
- [41] N. Zwettler, J.A. Schachner, F. Belaj, N.C. Mosch-Zanetti, Oxorhenium(V) complexes with phenolate-pyrazole ligands for olefin epoxidation using hydrogen peroxide, *Inorg. Chem.* 53 (2014) 12832.
- [42] J. Jacob, I.A. Guzei, J.H. Espenson, Synthesis, structure, and reactivity of novel dithiolato(oxo)rhenium(V) complexes, *Inorg. Chem.* 38 (1999) 1040.
- [43] P.D. Benny, J.L. Green, H.P. Engelbrecht, C.L. Barnes, S.S. Jurisson, Reactivity of rhenium(V) oxo schiff base complexes with phosphine ligands: rearrangement and reduction reactions, *Inorg. Chem.* 44 (2005) 2381.
- [44] I. Gryca, B. Machura, L.S. Shul'pina, G.B. Shul'pin, Synthesis, structures and catalytic activity of p-tolylimido rhenium(V) complexes incorporating quinolone-derived ligands, *Inorg. Chim. Acta* 455 (2016) 683.